Wettability of Zinc Oxide Surfaces with Controllable Structures

ARTICLE *in* LANGMUIR · MARCH 2006

Impact Factor: 4.46 · DOI: 10.1021/la053428q · Source: PubMed

3 AUTHORS, INCLUDING:

Weihuan Huang
Petrochemical Research Institute, Petrochin…
20 PUBLICATIONS **387** CITATIONS

SEE PROFILE

Wettability of Zinc Oxide Surfaces with Controllable Structures

Jilin Zhang, Weihuan Huang, and Yanchun Han*

State Key Laboratory of Polymer Physics and Chemistry, Changchun Institute of Applied Chemistry, Chinese Academy of Sciences, Graduate School of the Chinese Academy of Sciences, Changchun 130022, PR China

Received December 19, 2005. In Final Form: February 15, 2006

Zinc oxide (ZnO) surfaces with controllable structures (i.e, microstructure, nanostructure, and micronanobinary structure) have been created by controlling pH at <4 or >10.5 in the Zn(gray) + H_2O_2 reaction. The resulting surface shows superhydrophobicity. It is found that the water contact angle (CA) of the surface with micronanobinary structure is greater than that of nanostructure and that of nanostructure is greater than that of the microstructure. Theoretical analysis is completely in agreement with the experimental results.

Introduction

Wettability is an important property of solid materials and is governed by both the surface chemical composition and the surface geometrical structure.[1−4] In the past few years, the fabrication of super-water-repellent or superhydrophobic surfaces, with a water contact angle (WCA) greater than 150°, has attracted much interest because of the great practical applications in our life.[3] In general, the water contact angle on the smooth, known lowest-free-energy materials (i.e., fluorinated surface) is no more than 120°. However, some natural leaves, such as lotus leaves having WCA values as high as 160° or above are due to the surface micronanobinary structure.[5] That means that surface roughness plays an important role in determining the wetting behavior of solid surfaces. Accordingly, most of the artificial superhydrophobic surfaces are prepared by combining appropriate surface roughness with low-surface-energy materials.[6−19] For example, Jiang's group prepared super-water-repellent polyacrylonitrile (PAN)[7a] and poly(vinly alcohol) (PVA)[7b] films with nanometer-scale fibrous structures. Xu's group fabricated superhydrophobic micronanobinary structure polymer films by taking advantage of copolymer micellar aggregates in the selective solvent[8a] and polymer-phase separation in selective solvent vapor during the solidifying process.[8b] Shirtcliffe et al. prepared the dual-scale roughness superhydrophobic copper surfaces by the electrodepositing method.[9a] Zhang's group fabricated superhydrophobic self-assembled monolayer (SAM) films by utilizing electrochemical deposition and layer-by-layer (LbL) methods to self-assemble thiol molecules on gold and silver with micronanobinary structure[10] and so forth.[11−20] It is well known that micro- and nanostructures are essential for superhydrophobicity.[6] However, there are still some questions that need to be discussed, such as, what is the relationship between surface wettability and surface structures? Why does the micronanobinary structure improve the surface hydrophobicity to the greatest extent?

Herein, zinc oxide (ZnO) surfaces with controllable structures (i.e, microstructure, nanostructure, and micronanobinary structure) have been created by controlling pH at <4 or >10.5 in the Zn(gray) + H_2O_2 reaction. The resulting surface shows superhydrophobicity. It is found that the WCA of the surface follows the order $WCA_{micronanobinary} > WCA_{nanostructure} > WCA_{microstructure}$. Theoretical analysis is completely in agreement with the experimental results.

Experimental Section

Zinc power (0.65 g) and 30% hydrogen dioxide (H_2O_2) solution (10 g, the fraction of H_2O_2 solution is superfluous) were mixed and stirred. They were put into five conical flasks A−E. For A and B, acetic acid (HAc) was added to tune the pH values to ∼2.5 and 4, respectively. For D and E, ammonia (NH_3H_2O) was added to control the pH values at ∼9 and 10.5, respectively. After 5, 24, and 48 h,

* To whom correspondence should be addressed. E-mail: ychan@ciac.jl.cn. Tel: +86-431-5262175. Fax: +86-431-5262126.

(1) (a) Herminghaus, S. *Europhys. Lett.* **2000**, *52*, 165. (b) Abbott, N. L.; Folkers, J. P.; Whitesides, G. M. *Science*, **1992**, *257*, 1380. (c) Bico, J.; Tordeux, C.; Quéré, D. *Europhys. Lett.* **2001**, *55*, 214. (d) Callies, M.; Quéré, D. *Soft Mater*. **2005**, *1*, 55. (e) Lenz, P. *Adv. Mater.* **1999**, *11*, 1531.

(2) (a) Shull, K. R.; Karis, T. E. *Langmuir* **1994**, *10*, 334. (b) Hui, M.; Blunt, M. J. *J. Phys. Chem. B* **2000**, *104*, 3833. (c) Yoo, D.; Shiratori, S. S.; Rubner, M. F. *Macromolecules* **1998**, *31*, 4309.

(3) (a) Onda, T.; Shibuichi, S.; Satoh, N.; Tsujii, K. *Langmuir* **1996**, *12*, 2125. (b) Shibuichi, S.; Onda, T.; Satoh, N.; Tsujii, K. *J. Phys. Chem.* **1996**, *100*, 19512. (c) Chen, W.; Fadeev, Y.; Heieh, M. C.; Öner, D.; Youngblood, J.; McCarthy, T. J. *Langmuir* **1999**, *15*, 3395. (d) Öner, D.; McCarthy, J. *Langmuir* **2000**, *16*, 7777. (e) Nakajima, A.; Hashimoto, K.; Watanabe, T. *Monatsh. Chem.* **2001**, *132*, 31.

(4) (a) Zhang, J.; Xue, L.; Han, Y. *Langmuir* **2005**, *21*, 5. (b) Nakae, H.; Inui, R.; Hirata, Y.; Satio, H. *Acta Mater*. **1998**, *46*, 2313.

(5) Barthlott, W.; Neinhuis, C. *Planta* **1997**, *202*, 1.

(6) Sun, T.; Feng, L.; Gao, X.; Jiang, L. *Acc. Chem. Res.* **2005**, *38*, 644.

(7) (a) Feng, L.; Li, S. H.; Li, H. J.; Zhai, J.; Song, Y. L.; Jiang, L.; Zhu, D. B. *Angew. Chem., Int. Ed.* **2002**, *41*, 1221. (b) Feng, L.; Song, Y.; Zhai, J.; Liu, B.; Xu, J.; Jiang, L.; Zhu, D. *Angew. Chem., Int. Ed.* **2003**, *42*, 800. (c) Feng, L.; Li, S. H.; Li, Y. S.; Li, H. J.; Zhang, L. Z.; Zhai, J.; Song, Y. L.; Liu, B. Q.; Jiang, L.; Zhu, D. B. *Adv. Mater.* **2002**, *14*, 1857. (d) Jiang, L.; Zhao, Y.; Zhai, J. *Angew. Chem., Int. Ed*. **2004**, *43*, 4338. (e) Gao, X.; Jiang, L. *Nature* **2004**, 36.

(8) (a) Xie, Q.; Fan, G.; Zhao, N.; Guo, X.; Xu, J.; Dong, J.; Zhang, L.; Zhang, Y.; Han, C. C. *Adv. Mater*. **2004**, *16*, 1830. (b) Zhao, N.; Xu, J.; Xie, Q.; Weng, L.; Guo, X.; Zhang, X.; Shi, L. *Macromol. Rapid Commun*. **2005**, *26*, 1075.

(9) (a) Shirtcliffe, N. J.; McHale, G.; Newton, M. I.; Chabrol, G.; Perry, C. C. *Adv. Mater*. **2004**, *16*, 1929. (b) McHale, G.; Shirtcliffe, N. J.; Aqil, S.; Perry, C. C.; Newton, M. I. *Phys. Rev. Lett.* **2004**, *93*, 036102. (c) McHale, G.; Shirtcliffe, N. J.; Newton, M. I. *Langmuir* **2004**, *20*, 10146.

(10) (a) Jiang, Y.; Wang, Z.; Yu, X.; Shi, F.; Xu, H.; Zhang, X. *Langmuir* **2005**, *21*, 1986. (b) Zhang, X.; Shi, F.; Yu, X.; Liu, H.; Fu, Y.; Wang, Z.; Jiang, L.; Li, X. *J. Am. Chem. Soc.* **2004**, *126*, 3064. (c) Yu, X.; Wang, Z.; Jiang, Y.; Shi, F.; Zhang, X. *Adv. Mater.* **2005**, *17*, 1289.

(11) Erbil, H. Y.; Demirel, A. L.; Avci, Y.; Mert, O. *Science* **2003**, *299*, 1377.

(12) Hosono, E.; Fujihara, S.; Honma, I.; Zhou, H. *J. Am. Chem. Soc.* **2005**, *127*, 13458.

(13) Shiu, J.; Kuo, C.; Chen, P.; Mou, C. *Chem. Mater*. **2004**, *16*, 561.

(14) Minko, S.; Müller, M.; Motornov, M.; Nitschke, M.; Grundke, K.; Stamm, M. *J. Am. Chem. Soc.* **2003**, *125*, 3896.

(15) Nakajima, A.; Fujishima, A.; Hashimoto, K.; Watanabe, T. *Adv. Mater*. **1999**, *11*, 1365.

(16) Han, J. T.; Lee, D. H.; Ryu, C. Y.; Cho, K. *J. Am. Chem. Soc.* **2004**, *126*, 4796.

(17) Yabu, H.; Takebayashi, M.; Tannaka, M.; Shimomura, M. *Langmuir* **2005**, *21*, 3235.

(18) Han, J. T.; Xu, X.; Cho, K. *Langmuir* **2005**, *21*, 6662.

(19) Lau, K. K. S.; Bico, J.; Teo, K. B. K.; Chhowalla, M.; Amaratunga, G. A. J.; Milne, W. I.; Mckinley, G. H.; Gleason, K. K. *Nano Lett.* **2003**, *3*, 1701.

(20) (a) Zhang, J.; Li, J.; Han, Y. *Macromol. Rapid Commun.* **2004**, *25*, 1105. (b) Lu, X.; Zhang, C.; Han, Y. *Macromol. Rapid Commun*. **2004**, *25*, 1606.

10.1021/la053428q CCC: $33.50
Published on Web 03/07/2006

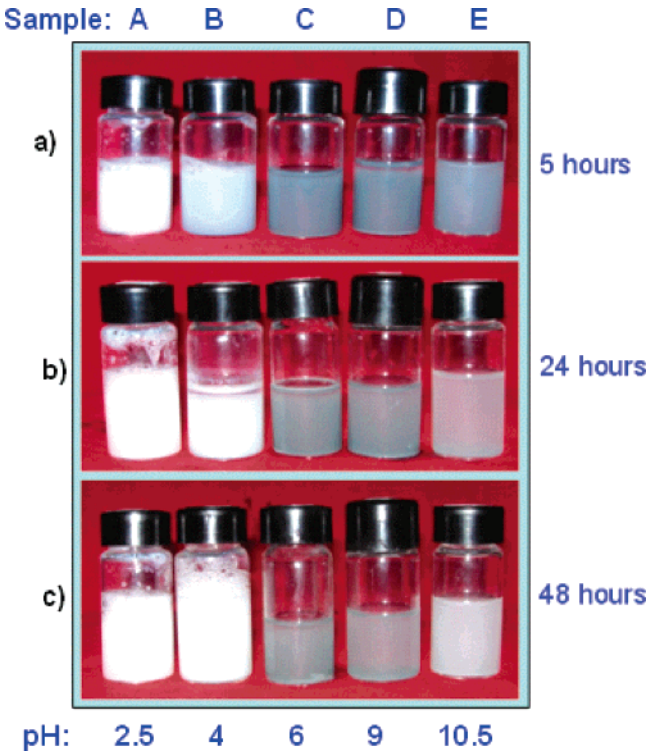

Figure 1. Photographs of the products of the Zn(gray) + H_2O_2 reaction at different pH values for (a) 5, (b) 24, and (c) 48 h, respectively: (A) pH 2.5, (B) pH 4, (C) pH 6, (D) pH 9, and (E) pH 10.5.

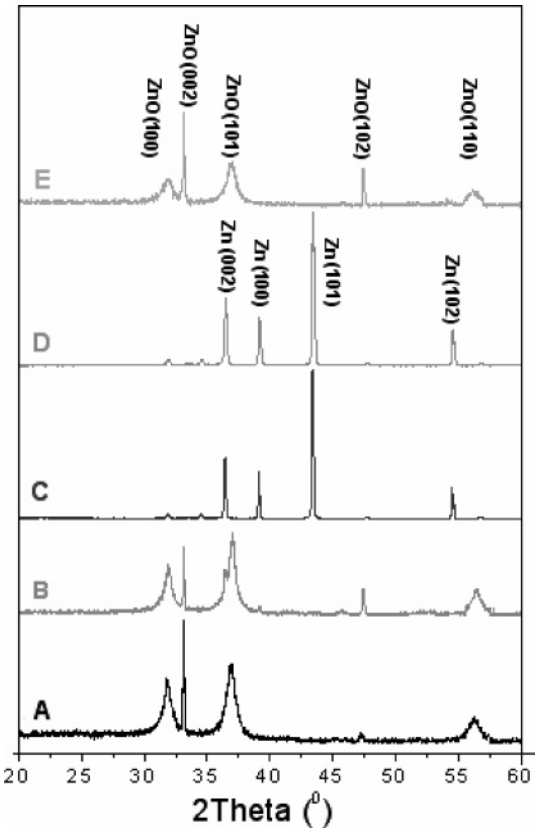

Figure 2. XRD patterns of products A−E: (A) ZnO, (B) ZnO, (C) Zn, (D) Zn, and (E) ZnO.

photographs of A−E were taken. The final products of A−E (A and B after 5 and 24 h of reaction, respectively, and C−E after 240 h of reaction) were thoroughly rinsed with deionized water. The aqueous

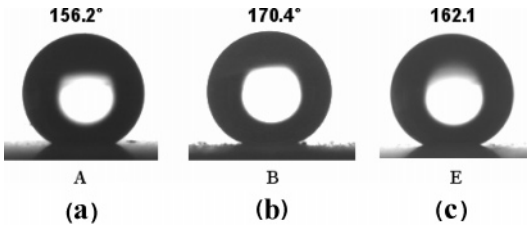

Figure 3. Water contact angles for A, B, and E film final products. (a) A: 156.2 ± 1.2°; (b) B: 170.4 ± 0.7°; and (c) E: 162.1 ± 1.7°.

Table 1. Reaction Conditions and Respective Products of SamplesA−E

sample	A	B	C	D	E
catalyzer	HAc	HAc	nothing	NH_3H_2O	NH_3H_2O
pH value	2.5	4	6	9	10.5
reaction time (h)	5	24	240	240	240
product	ZnO	ZnO	Zn	Zn	ZnO

product suspensions were then dropped onto the cleaned silicon wafer (cleaned with a 70/30 v/v solution of 98% H_2SO_4/30% H_2O_2 at 80 °C for 30 min and then thoroughly rinsed with deionized water and dried) to dry at atmospheric conditions. After that, all of the products were heated and held at 100 °C in a vacuum for 24 h to remove the residual water, and then they were used to obtain the X-ray diffraction spectrum (XRD), the water contact angle (WCA), and the field emission scanning electronic microscope (FESEM) characterization.

The XRD pattern was collected on a Rigaku-Dmax 2500 diffractometer using Cu Kα radiation (0.15405 nm). Contact angles were determined using a Krüss DSA10-MK2 (Germany) contact angle measuring system at ambient temperature. The probe fluid was deionized water, and the droplet volume was 5 μL. The average CA value was obtained by measuring the same sample at 10 different positions. The microstructures of the films were investigated with a Micro FEI Philips XL-30-ESEM-FEG scanning electronic microscope (FESEM) operating at 20 kV.

Results and Discussion

The oxidation ability of H_2O_2 on zinc is dependent on pH. Under neutral or alkalescent conditions, zinc cannot be oxidized by H_2O_2 (eq 1). However, at acidic or alkaline conditions, oxidation occurs because the H^+ and OH^- ions catalyze the reaction (eq 2).[21]

$$\mathrm{Zn(gray) + H_2O_2} \xrightarrow{\mathrm{pH} \sim 7} \text{no reaction} \qquad (1)$$

$$\mathrm{Zn(gray) + H_2O_2} \xrightarrow{4 \geq \mathrm{pH} \geq 11} \mathrm{ZnO(white) + H_2O} \qquad (2)$$

Figure 1 shows the photos of products of the Zn(gray) + H_2O_2 reaction under different pH conditions for (a) 5, (b) 24, and (c) 48 h, respectively, at (A) pH 2.5, (B) pH 4, (C) pH 6, (D) pH 9, and (E) pH 10.5. The reaction and reaction velocity both depend on the catalyzer concentration (i.e., pH value). After 5 h, sample A (pH ∼2.5) reacted completely (Figure 1a). Sample B reacted almost completely after 24 h, whereas the reaction of sample E (pH ∼10.5) just began (Figure 1b) and was complete after 240 h. Samples C (pH ∼6) and D (pH ∼9) did not react at all even after 240 h.

Figure 2 shows the XRD spectra of the final products of A−E. The peaks at 32, 33, 37, 47.5, and 56° (Figure 2a, b, and e) correspond to the ZnO(100), (002), (101), (102), (110) plane,

(21) The catalysis reactions can be shown below: under acidic conditions, the cathode reaction is Zn(s) + H_2O(l) − 2e → ZnO(s) + $2H^+$, and the anode reaction is H_2O_2(l) + $2H^+$ + 2e → $2H_2O$. Under basic conditions, the cathode reaction is Zn(s) + $2OH^-$ − 2e → ZnO(s) + H_2O(l), and the anode reaction is H_2O_2(l) + 2e → $2OH^-$.

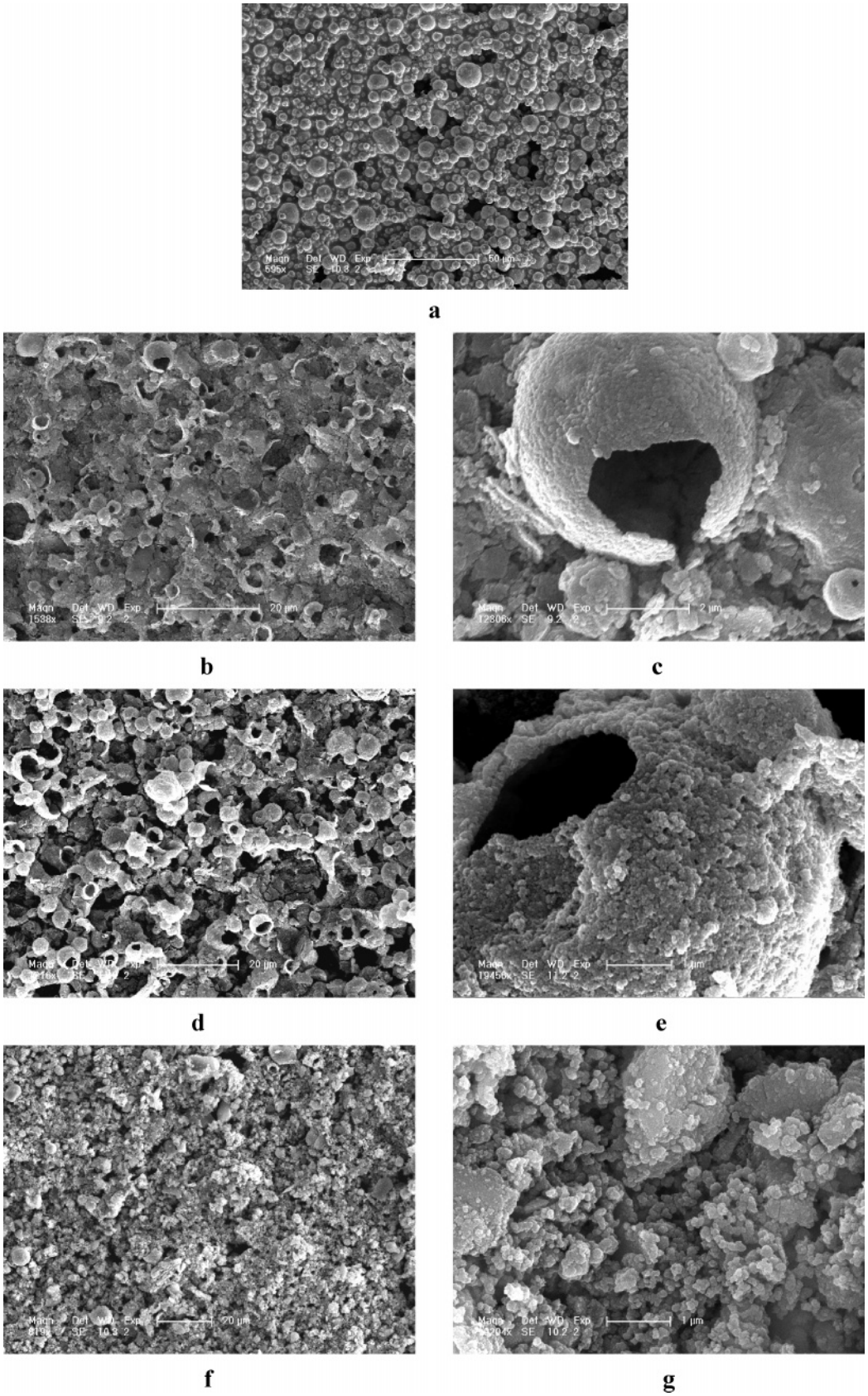

Figure 4. Typical FESEM images of A, B, C, and E film final products. (a) C: sphere structure of Zn power and overview and magnification of ZnO; (b, c) A: microscale hollow sphere structure dominated; (d, e) B: micronanobinary structure (microscale hollow sphere and nanoscale protrusion binary structure); and (f, g) E: nanoscale protrusion structure dominated.

which proves that samples A, B, and E have reacted completely and the product is ZnO. The peaks at 36.5, 39, 43, and 54.5° (Figure 2c and d) correspond to the Zn(002), (100), (101), (102) plane, which proves that samples C and D do not react at all. The reaction conditions and the products of each sample are listed in Table 1.

At ambient conditions, ZnO is not hydrolytic because of its good chemical stability. ZnO is a hydrophobic material with WCA $\approx 110°$ on the flat surface.[22] Herein, the products of A, B, and E all show superhydrophobicity, and the WCAs are $156 \pm 1.2°$, $170.4 \pm 0.7°$, and $162.1 \pm 1.7°$, respectively (Figure 3). Why do these ZnO films show super water repellency but with different WCAs? It is believed to be due to the surface structures.

The structures of each sample are investigated by FESEM (Figure 4). Figure 4a shows the product of sample C (i.e., Zn power with a spherical structure). Figure 4b and c shows the microstructure of the product of sample A, which is dominated by microscale hollow spheres. The average particle radius ($r = \Sigma r_i/n$) is around 1.00 μm. In Figure 4c, it can be found that the hollow-sphere surfaces are relatively smooth and that there are fewer nanoscale protrusions on them. However, Figure 4d and e shows that the product of sample B has both microscale hollow-sphere structure and nanoscale protrusion structure on the hollow-sphere surfaces (i.e., the product of sample B is dominated by micronanobinary structure). The surface of sample E is relatively smooth on the micrometer scale and is dominated by nanoscale protrusion structure. The average particle radius ($r' = \Sigma r_i/n$) is around 0.10 μm (Figure 4f and g).

The reaction mechanisms of Zn(gray) + H_2O_2 at different pH values may help us to understand the reason that the products of A, B, and E have different structures. Among the five samples, sample A has the highest reaction velocity (<5 h) because of the higher concentration of the catalyzer (i.e., H^+). Such a high reaction velocity prevented the formation of ZnO nanocrystals. Correspondingly, the product lacks nanoscale protrusion structure. However, sample E has the lowest reaction velocity (>200 h). The unstable hollow-sphere structure can be destroyed completely during such a long reaction period. Thus, the structure of the product of sample E is dominated by nanoscale ZnO crystals. Compared with samples A and E, sample B has the appropriate reaction velocity (~24 h), which is suitable for preserving the unstable microscale hollow-sphere structure and forming nanoscale ZnO crystals. Therefore, this is the reason that the product of sample B has micronanobinary structures.

In general, surface roughness is considered to be the key factor affecting surface wettability. The wettability of a surface can be enhanced by increasing the surface roughness within a special size range[1,24,25] because the air trapped between the solid surface and the water droplet can minimize the contact area. The relationship between the surface wettability and the surface roughness can be well described by the Cassie equation (eq 3).[24]

$$\cos\theta_r = f_1 \cos\theta - f_2 \tag{3}$$

Here, θ_r and θ are the CAs on ZnO with rough and smooth surfaces, respectively. f_1 and f_2 are the fractional interfacial areas of ZnO and the air trapped between the ZnO surface and a water droplet, respectively (i.e., $f_1 + f_2 = 1$). This equation indicates that the larger air fraction (f_2), the more hydrophobic the surface. In our experiment, both microscale hollow-sphere structures and nanoscale protrusion structures can bring a large quantity of trapped air when in contact with water ($f_2(A) = 0.871$, $f_2(B) = 0.982$, and $f_2(E) = 0.926$, calculated from experimental results), which is essential for ZnO films (samples A, B, and E) showing super water repellency. Interestingly, although both microstructure and nanostructure can change the surface roughness, which one is better and which structure can improve the surface hydrophobicity the greatest has not yet been systemically explored. Our experimental results indicate that the micronanobinary structure has the greatest ability to increase the surface superhydrophobicity and the nanostructure is better than the microstructure at improving the surface superhydrophobicity.

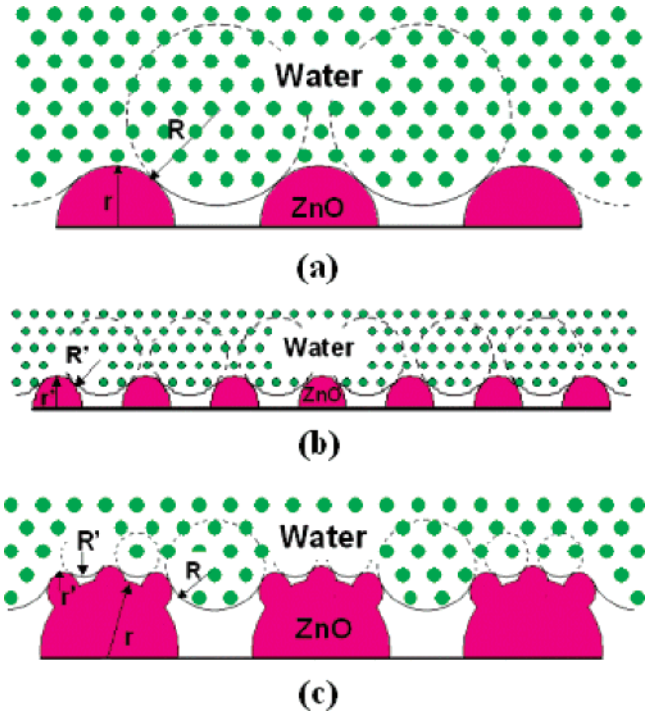

Figure 5. Schematic illustrations of the shapes of water on the surface with different structures. (a) A: microscale structure. (b) E: nanoscale structure. (c) B: micronanobinary structure.

To thoroughly understand these phenomena, theoretical considerations are necessary. Figure 5 is the schematic illustration of the shapes of water for structured films on different scales. Herein, two parameters (i.e., the average curvature radius ($R = \Sigma R_i/n$) and average particle radius ($r = \Sigma r_i/n$) can affect the air fraction (f_2) of the surface). In our previous work[4a] and Nakae et al.'s work,[4b] R and f_2 can be roughly expressed by eqs 4 and 5.

$$R = A(1 - e^{-Br}) \tag{4}$$

$$f_2 = \frac{R}{R + r} = \frac{1}{\frac{r}{R} + 1} \propto \frac{R}{r} \tag{5}$$

Here, A is a function of θ. In our study, A is constant because the surface materials (ZnO) and the probe fluid (deionized water) are kept the same. The surface energy of a liquid (γ_L) and B are also constant. Equations 4 and 5 indicate that $f_2 \propto (R/r) \propto (1 - e^{-Br})/r$ and the derivative of df_2/dr can be expressed by eq 6.

$$\frac{df_2}{dr} \propto \frac{[(Br + 1)e^{-Br} - 1]}{r^2} \leq 0^{23} \tag{6}$$

The derivative of df_2/dr is always less than 0 (at $r > 0$), indicating that the surface air fraction (f_2) always decreases with an increase in the surface structure scale (r). The average particle radius of nanoscale protrusions ($r' = 0.10$ μm) is far less than that of a microscale hollow sphere ($r = 1.00$ μm) (i.e., $r' < r$, correspondingly, $f_2(E) > f_2(A)$). Therefore, this is the theoretical reason that the nanoscale protrusion structure has a greater increase

(22) Liu, H.; Feng, L.; Zhai, J.; Jiang, L.; Zhu, D. *Langmuir* **2004**, *20*, 5659.
(23) For $e^x > x + 1$ ($x > 0$), we have $(x + 1)e^{-x} < 1$, which means $(Br + 1)e^{-Br} - 1 < 0$.
(24) Cassie, A. B. D. *Discuss. Faraday Soc.* **1948**, *3*, 11.
(25) Wenzel, R. N. *Ind. Eng. Chem.* **1936**, *28*, 988.

Table 2. Water Contact Angles, Dominated Surface Structures, and f_2 Values of Samples A−E

sample	A	B	E
contact angle (deg)	156.2	170.4	162.1
structure scale	micrometer	micronanometer	nanometer
f_2 (exptl)	0.871	0.982	0.926
$\boldsymbol{r}$ (μm)	1.00	1.00	non
$\boldsymbol{R}$ (μm)	6.70	6.70	non
$\boldsymbol{r'}$ (μm)	non	0.10	0.10
$\boldsymbol{R'}$ (μm)	non	1.33	1.33
f_2 (theor)	$R/(R + r) = 0.870$	$(R + R')/(R + R' + r') = 0.986$	$R'/(R' + r') = 0.930$
hydrophobicity increase		sample B > sample E > sample A	

in surface superhydrophobicity than the microscale structure. Constants A and B are calculated to be 8.00 μm and 1.82×10^6 μm^{-1}, and R and R' are 6.70 and 1.33 μm, respectively.[26] Given by the values of A, B, r, r', R, and R', the theoretical f_2 values for the three different structure surfaces have been calculated and listed in Table 2. The theoretical results are in good agreement with the experimental results, which means that our hypothetical model can well explain this wetting phenomenon. It is found that $f_2(B) = 0.986 > f_2(E) = 0.930 > f_2(A) = 0.870$, which means that the micronanobinary structure has the greatest ability to increase the surface superhydrophobicity and the nanostructure is better than the microstructure at improving the surface superhydrophobicity. Our experimental results are in good agreement with the theoretical conclusions.

(26) Given by the experimental results (samples A and E) $r \approx 1.0$ μm, $r' \approx 0.10$ μm, $f_2(A)_{exptl} \approx 0.871$, and $f_2(E)_{exptl} \approx 0.926$, the value of $e^{-Br'} \approx 0.8338$ can be calculated by the following equation: $e^{-10Br'} = 5.04e^{-Br'} - 4.04$. Therefore, $B = 1.82 \times 10^6$ μm^{-1} and $A = 8.00$ μm.

Conclusions

Zinc oxide (ZnO) surfaces with controllable structures (i.e, microstructure, nanostructure, and micronanobinary structure) have been created by controlling pH at <4 or >10.5 in the Zn(gray) + H_2O_2 reaction. The resulting surfaces show superhydrophobicity with water contact angles in the following order: $WCA_{micronanobinary\ structure} > WCA_{nanostructure} > WCA_{microstructure}$. Theoretical analysis is completely in agreement with the experiment results.

Acknowledgment. This work was subsidized by the National Natural Science Foundation of China (grants 50125311, 20334010, 20274050, 50390090, 50373041, 20490220, 20474065, 50403007, and 50573077), the Ministry of Science and Technology of China (grant 2003CB615601), the Chinese Academy of Sciences (Distinguished Talents Program, grant KJCX2-SW-H07), and the Jilin Distinguished Young Scholars Program (grant 20010101).

LA053428Q